Paradigm Academic Press
Innovation in Science and Technology
ISSN 2788-7030
JAN. 2024 VOL.3, NO.1

Modelling and Simulation of the Strength Properties of Ultra-High Performance Fiber Reinforced Concrete Specimens

A. S. J. Smith[1] & G. M. S. Islam[1]

[1] College of Civil Engineering and Architecture, China Three Gorges University, Yichang 443002, China

Correspondence: A. S. J. Smith, College of Civil Engineering and Architecture, China Three Gorges University, Yichang 443002, China.

doi:10.56397/IST.2024.01.01

Abstract

The strength performance of UHPFRC with micro and hooked-ends steel fibers was studied in this paper using Finite Element (FE) modelling and simulation. The specimens were modelled in geometry, material, constraints, load and boundary conditions using ABAQUS package and dynamic explicit analysis was used to investigate the crack pattern, failure mode and stress-stain behaviour of the UHPFRC specimens when subjected to uniaxial compression and tension loading. Results from the FE simulation revealed that the surfaces of the UHPFRC specimens were still in good shape after attaining their ultimate resistance against compression and tension loading. The UHPFRC's ultimate compressive strength of 260N/mm2 was just 7% higher than the experimental compressive strength. The UHPFRC exhibited both linear compressive stress-strain behaviour up to 89% of its peak strength and non-linear stress-strain behaviour with strain hardening and strain softening phases. Further findings also showed that the UHPFRC despite having ultra-high tensile strength did not undergo strain hardening phase as the vertical direction stresses were mainly distributed around the loaded section of the specimen. The FE UHPFRC models' strength in compression and tension only has slight and negligible variations from the experimental strengths. The deformation and strength performance of the FE specimens are in perfect agreement with the experimental specimens. Therefore, FE modelling and simulation can be used as a reliable method of carrying out extensive studies on UHPFRC properties and performances.

Keywords: modelling, simulation, strength properties, ultra-high performance fiber reinforced concrete

1. Introduction

Ultra-high performance fiber reinforced concrete (UHPFRC) is a concrete that has a compressive strength of at least 150N/mm^2 (AFGC, 2002) with better performance in strength, durability and rheology when compared with normal strength concrete (NSC) (Azmee & Shafiq, 2018). The ultra-high strength of UHPFRC is a result of its ingredients which include high cement content, powder like silica fume, very fine aggregate like quartz sand, steel fibers, super plasticizer and a very low water-cement ratio (w/c) (Raja & Sujatha, 2014; Sadrekarimi, 2004). Researchers are now intensifying interest in the investigation of UHPFRC properties as well as its structural performance because of its excellent properties. Many studies on the strength of UHPFRC have already been done by several researchers. For instance, Hashim et al. (2020) investigated the mechanical properties of UHPFRC containing different types of fiber and used the stress-strain results obtained to develop damage and constitutive models for UHPFRC. The models when employed in Finite Element Method (FEM) to simulate the load-displacement property of a hollow concrete column, yielded promising results. Graybeal and Baby (2013) studied the tensile strength property of UHPFRC and utilized the findings obtained to develop a direct method of testing the tensile property of UHPFRC. Findings from Graybeal and Baby showed that UHPFRC specimen subjected to direct tension test has four phases of tensile response: (1) elastic phase (2) multi-cracking phase (3) crack straining phase (4) localization phase. Krahl et al. (2018) conducted research on the mechanical properties

of UHPFRC and proposed a mechanical damage and stress-strain models using the obtained results. Verification of Krahl et al.'s models through numerical simulation showed good correlation. Prem et al. (2012) conducted research on UHPFRC to evaluate its mechanical properties and findings revealed that change in the volume of steel fiber and aspect ratio lead to substantial change in the strength properties of UHPFRC. There is no specific strength value for UHPFRC in compression or tension; and the values depend on the target strength, mix design and curing condition as researchers like Rossi et al. (2004) has reported that UHPFRC's compressive strength and tensile strength may even be as high as 204N/mm^2 and 20N/mm^2.

The cost of producing UHPFRC is very high when compared with NSC due to its special ingredients and testing conditions; and this high fund requirement has hindered researchers from carrying out aggressive experimental studies on UHPFRC. However, a less costly way (which researchers rarely take advantage of) of investigating the properties and performance of UHPFRC which produces highly correlated results with experimental results is Finite Element (FE) numerical modelling and simulation. Numerical modelling basically involves the modelling of UHPFRC's geometry, material (using mechanical properties obtained from experiment), constraints and boundary conditions. While numerical simulation involves the computer analysis (static or dynamic analysis depending on the property or behavior being investigated) of the UHPFRC specimen's property or element's performance. The use of FE model to study UHPFRC properties is not straight forward as it requires the use of damage and stress-strain models peculiar to UHPFRC to model its material properties; and this may also be one of the reasons why there are limited studies in this area but many researchers have developed models that can be used to capture the damage of UHPFRC under compressive and tensile loading as well models that can be used to predict its stress-strain response. For instance, Tian et al. (2023) studied the behavior of UHPFRC subjected to cyclic and monotonic tensile loading; and utilized the study findings to propose a tensile damage and stress-strain models for UHPFRC. Hashim et al. (2020) also proposed simplified damage plasticity and stress-strain models for UHPFRCs and findings revealed that the models perfectly predict the damage as well as the stress-strain behavior of the studied UHPFRC.

Many researchers have not shown much interest in using numerical modelling and simulation to study the properties of UHPFRC even though several literatures that employed the use of numerical simulation are available. Some of which include: Shi et al. (2023) study on the response and constitutive model of UHPFRC under tension loading whose numerical results showed good prediction of the UHPFRC's tensile stress-strain behavior. Bahraq et al. (2019) numerical research on the shear performance of reinforced concrete beams strengthened with UHPFRC in which the obtained failure mode and ultimate load matched perfectly with those obtained from experiment. The stress-strain behavior of UHPFRC subjected to uniaxial compression and tension was studied by Naeimi and Moustafa (2019) using DIANA package; and findings revealed that the experimental elastic and inelastic behaviors of the UHPFRC under both compression and tension were reproduced successfully through numerical modelling and simulation. Chowdhury et al. (2016) modelled steel fiber reinforced concrete (SFRC) cylinder and simulated its compressive and tensile properties using ANSYS package; and after deep analysis and optimization of the main parameters concluded that results from the numerical models have good correlation with the results from experiment.

Although some studies have been reported on numerical modelling and simulation of UHPFRC's properties, they are still far below the percentage of studies that should have been conducted using numerical simulation in order to understand the properties of UHPFRC that have not been studied due to the high cost of experimentation. So, the aim of this study is to investigate the compressive and tensile strength performance of UHPFRC with micro and hooked-ends steel fibers using FEM and to also check its performance variation level from that obtained through experiment.

2. Modelling

ABAQUS package was used to model and simulate the compressive and tensile properties of the UHPFRC specimens. The UHPFRC cube specimen of 100x100x100mm^3 in dimension, prism specimen of 100x100x300mm^3 in dimension and dog-bone specimen with length of 200mm, 50mmx50mmx25mm end sections, 26mmx50mm middle portion, 12mm length tapered section with a radius of 12mm, 126mm length notched cross-section were modelled using the three dimensional (3D), solid elements with three degrees of freedom (DOF) at each of its 8-nodes. The geometry of the specimens is presented in Figure 1.

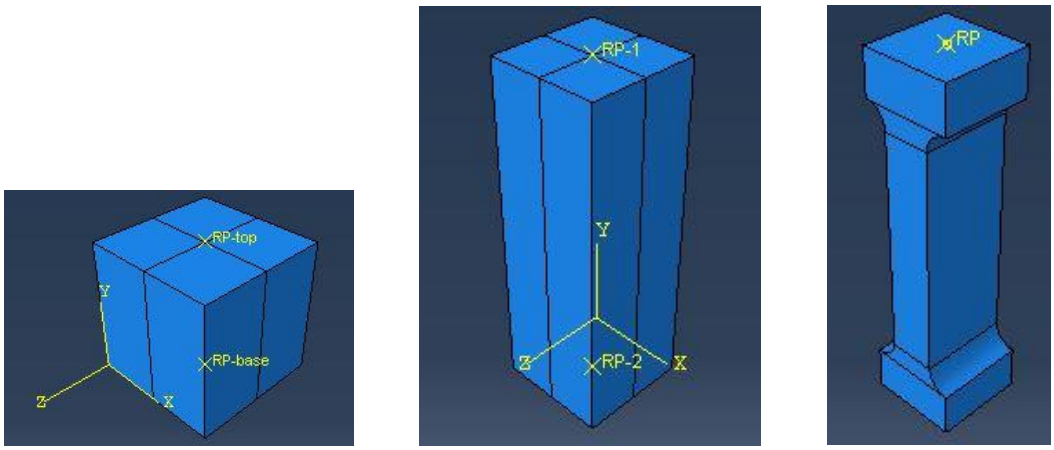

(a) Cube geometry (b) Prism geometry (c) Dog-bone geometry

Figure 1. Specimens' geometry

The UHPFRC material was modelled using concrete damage plasticity model (CDPM) developed by Lubliner et al. (1989) and Hashim et al. (2020) stress-strain model as expressed in (1).

$$\sigma = (1-d)E_o(\varepsilon - \varepsilon^{pl}) \tag{1}$$

where σ is the stress in compression/tension, d is the damage variable in compression/tension, E_0 is the elastic modulus, ε is the total strain and ε^{pl} is the plastic strain.

The damage parameters in compression and tension used for representing crack formation in the specimens are expressed in (2)-(3) based on Tao and Chen (2015) and Birtel and Mark (2006):

$$d_c = 1 - \frac{\sigma_c E_c^{-1}}{\varepsilon_c^{pl}\left(\frac{1}{b_c}-1\right)+\sigma_c E_c^{-1}} \quad or \quad d_c = 1 - \frac{\sigma_c E_c^{-1}}{\varepsilon_c^{in}(1-b_c)+\sigma_c E_c^{-1}} \tag{2}$$

$$d_t = 1 - \frac{\sigma_t E_t^{-1}}{\varepsilon_t^{pl}\left(\frac{1}{b_t}-1\right)+\sigma_t E_c^{-1}} \quad or \quad d_t = 1 - \frac{\sigma_t E_t^{-1}}{\varepsilon_t^{in}(1-b_t)+\sigma_t E_c^{-1}} \tag{3}$$

$$\varepsilon_c^{pl} = \varepsilon_c^{in} - \frac{d_c \sigma_c}{(1-d_c)E_o} \tag{4}$$

$$\varepsilon_t^{pl} = \varepsilon_t^{cr} - \frac{d_t \sigma_t}{(1-d_t)E_o} \tag{5}$$

$$\varepsilon_c^{in} = \varepsilon_c - \varepsilon_c^{el} \quad or \quad \varepsilon_c - \frac{\sigma_c}{E_o} \tag{6}$$

$$\varepsilon_t^{cr} = \varepsilon_t - \varepsilon_t^{el} \quad or \quad \varepsilon_t - \frac{\sigma_t}{E_o} \tag{7}$$

where d_c is compressive damage parameter which ranges from 0 to 1, d_t is tensile damage parameter which ranges from 0 to 1, σ_c is compressive stress of concrete, σ_t is tensile stress of concrete, E_o is modulus of elasticity of concrete, ε_c is total concrete strain in compression, ε_t is total concrete strain in tension, ε_c^{pl} is plastic strain corresponding to compressive strength of concrete, ε_t^{pl} is plastic strain corresponding to tensile strength of concrete, ε_c^{el} is elastic strain of concrete in compression, ε_t^{el} is elastic strain of concrete in tension, ε_c^{in} is inelastic strain of concrete in compression, ε_t^{cr} is cracking strain of concrete in tension, b_c and b_t are constant parameters with values $0 < b_c, b_t \leq 1$ ($b_c = 0.7$ and $b_t = 0.1$).

The UHPFRC's material used for tensile strength simulation was also modelled using ductility damage to show its damage evolution in terms of deformation and the variable employed for the ductility damage is shown in Table 2. The mechanical properties of the UHPFRC based on Hashim et al. (2020) and other modelling parameters are presented in Table 1:

Table 1. UHPFRC's mechanical and other modelling parameters

Compressive strength (N/mm^2)	242.6
Tensile strength (N/mm^2)	9.34
Elastic modulus (N/mm^2)	30000

Poisson's ratio	0.2
Dilation angle	33
Eccentricity	0.1
Density (kg/mm^3)	2.5E-9
fb0/fc0	1.16
k	0.67

Table 2. UHPFRC's ductility damage parameters

Fracture strain	Stress triaxiality	Strain rate
0.8709	0.0532	0.006
1.1739	0.4588	0.006

The top and bottom faces of the cube specimen were modelled with rigid body constraint; while the dog-bone specimen was modelled using coupling constraint. In terms of load and boundary conditions, fixed support was applied to the base of the cube and prism while vertical displacement load was applied to the top of the cube and prism using dynamic explicit analysis as shown in Figures 2(a-c). Vertical displacement load was applied at the top face of the dog-bone specimen using dynamic explicit analysis as shown in Figure 2(d); while the bottom cell of the dog-bone specimen was modelled with a fixed boundary condition and the top end section was modelled with vertical DOF as shown in Figure 2(d).

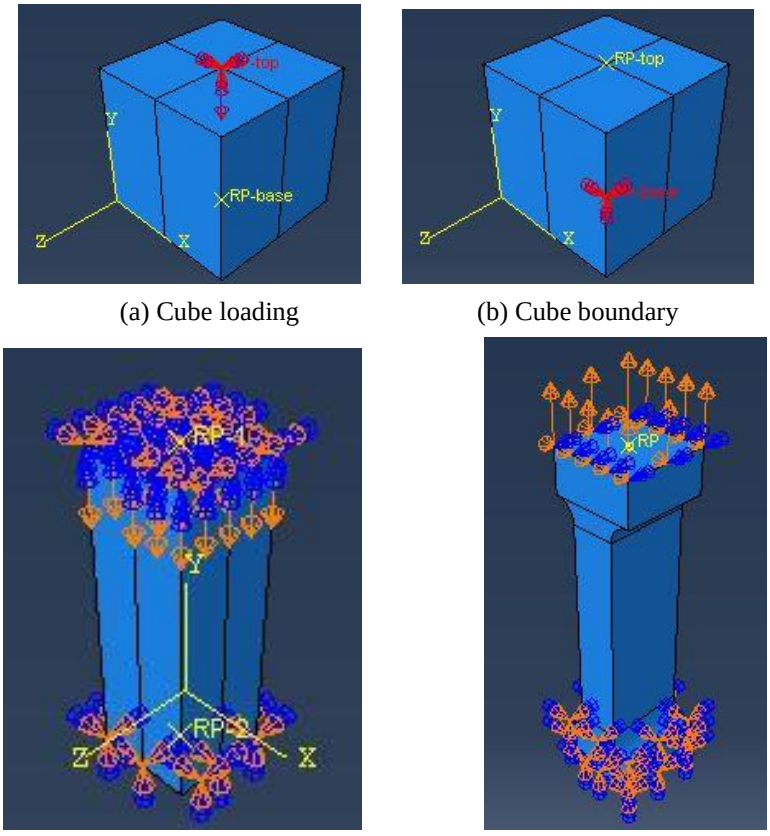

(a) Cube loading (b) Cube boundary

(c) Prism's load and boundary condition (d) Dog-bone load and boundary condition

Figure 2. Load and boundary conditions

The cube specimen, prism specimen and dog-bone specimen were meshed using mesh size of 10mm, 20mm and 6mm respectively; and the dog-bone specimen's end sections were assigned a local seed of 3mm to prevent element meshing error which usually leads to abortion of analysis. The meshed specimens are shown in Figure 3.

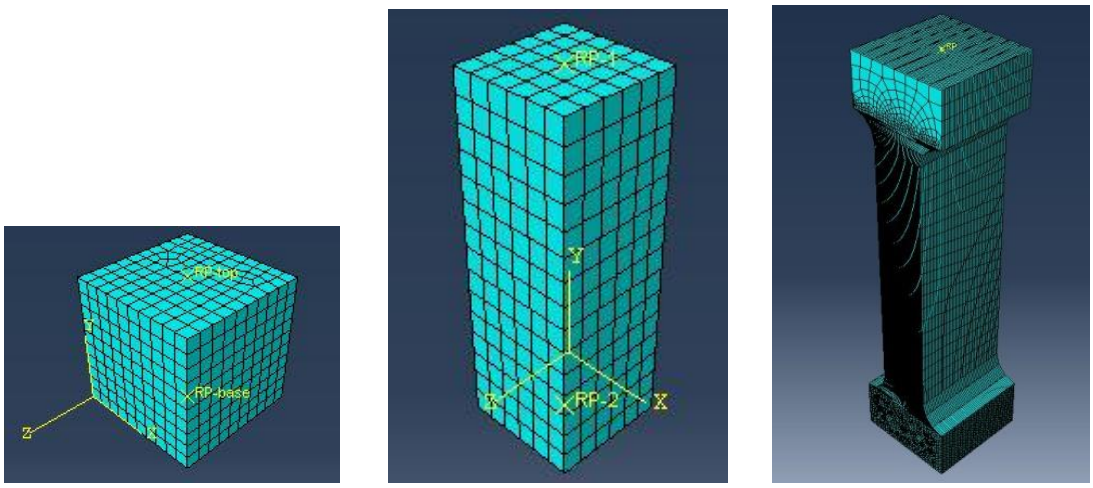

(a) Cube (b) Prism (c) Dog-bone

Figure 3. Meshed specimens

3. Results and Discussions

3.1 UHPFRC Specimens' Crack Pattern

The UHPFRC cube's cracks as can be seen in Figure 4(a) only became visible at its ultimate load as the specimen only underwent little deformation even after the applied load exceeded its ultimate resistance. The cube specimen has a type 1 failure mode based on ASTM C39/C39M (2014) fracture mode with a concentrated deformation at the centre and cross-spread through faint diagonal cracks to the edges of the specimen. The crack pattern of the cube specimen revealed that the surfaces of the cube did not undergo serious damage after the applied compressive load exceeded its compressive resistance; and this is mainly due to the ultra-high compressive strength of the UHPFRC cube specimen. The prism's crack as shown in Figure 4(b) appeared at a compressive stress of 144.6N/mm^2 and the failure mode was more of a type 6 failure with the cracks occurring at the middle of the specimen instead of the top part. The surface of the prism specimen, just like it is common with UHPFRC specimens subjected to uniaxial compression load did not undergo severe damage like normal concrete specimen; and this is largely due to the high stiffness and post-peak strength capacity of the cube specimen in agreement with El-Helou et al. (2022) research findings. The dog-bone specimen illustrated in Figure 4(c) failed through crack formation at the end of the notched section of the specimen and the appearance of its cracks occurred at a stress of 7.05N/mm^2. Even after attaining its optimum tensile strength, the dog-bone specimen remained largely undamaged and this showed the high resistance of this UHPFRC to tensile deformation. This high resistance to tensile deformation exhibited by the dog-bone specimen is largely due to its high resistance to crack propagation and formation of new cracks during post-cracking phase, high strain capacity, and many discrete cracks that are pretty close to each other (El-Helou et al., 2022).

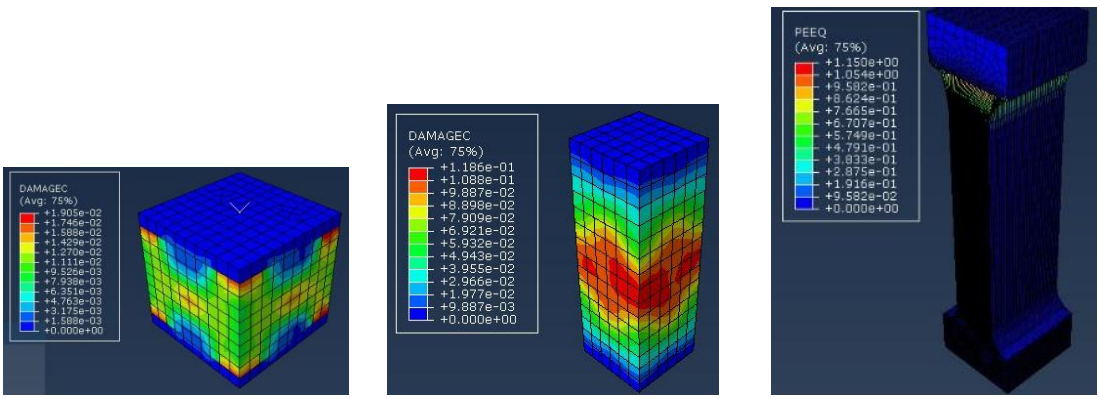

(a) Cube (b) Prism (c) Dog-bone

Figure 4. UHPFRC specimens' crack pattern

3.2 UHPFRC's Compressive and Tensile Strength

UHPFRC's ultimate compressive strength determine through the cube specimen is 260N/mm^2 and when compared with the 243N/mm^2 cylinder axial compressive strength reported by Hashim et al. (2020), the FE cube model's ultimate strength was 7% higher than the experimental strength. This increase is because cube specimens when subjected to compression load have more compression resistance than cylinder specimens due to their smaller dimensions. The stress-strain relationship as illustrated in Figure 5(a-b) showed that the FE prism specimen exhibited the same stress-strain behaviour like the experimental specimen having both elastic and plastic stages of deformation. The prism specimen's stress-strain behaviour was linear up to the stress of 190N/mm^2 and strain of 0.0065 even after crack appearance at a stress of 144.6N/mm^2 and strain of 0.00476; after which it became non-linear until the stress of 213N/mm^2 and strain of 0.01024. This means that the prism specimen's uniaxial compressive strength is 14% lower than the experimental uniaxial compressive strength; and this decrease is due to the slight difference in shape and size of the two specimens. The non-linearity of the prism specimen was characterised with some ductility property involving strain hardening behaviour up to its optimum compressive strength before the applied load exceeded its compressive resistance. The prism specimen was linear up to 89% of its peak strength and this can be comparable with the 90% linearity of the experimental specimen. This high linearity in its stress-strain is due to its ultra-high compressive strength in line with El-Helou et al. (2022) report that the high percentage of linearity of UHPFRC's stress-strain curve is mainly determined by its high compressive strength.

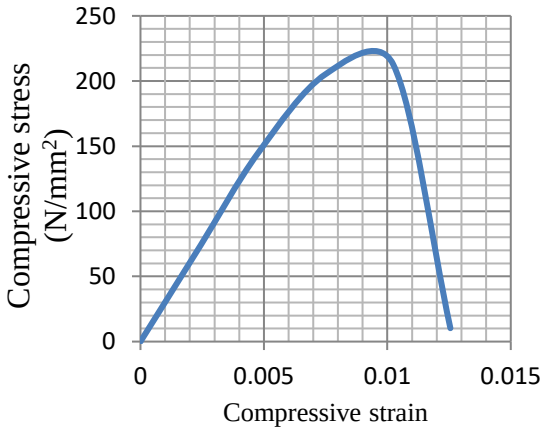

(a) FE prism model's compressive stress-strain

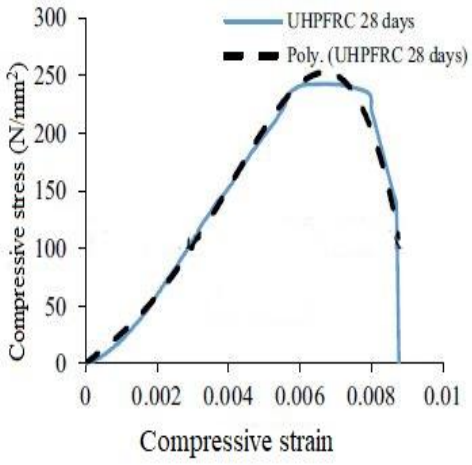

(b) Experimental compressive stress-strain (Hashim et al., 2020)

Figure 5. UHPFRCs' compressive stress-strain

The stress-strain relationship presented in Figures 6(a-b) revealed that the FE dog-bone specimen underwent similar deformation like the experimental dog-bone specimen. The FE dog-bone specimen has a linear stress-strain curve up to a tensile stress of 8.8N/mm^2 against the experimental tensile stress of 8.5N/mm^2; and this means that even after the appearance of crack in the critical section of the dog-bone specimen at 7.05N/mm^2

stress and 0.003 strain, the deformation of the specimen was still elastic. The FE dog-bone specimen's stress-strain behaviour became non-linear beyond the tensile stress of 8.8N/mm^2 until it attained its ultimate tensile strength of 9.33N/mm^2 at a strain of 0.008. The ultimate tensile strength of the FE dog-bone specimen was just 0.1% lower than the experimental ultimate tensile strength of 9.34N/mm^2; and this showed the high correlation between the FE model and the experimental specimen. The FE dog-bone specimen after attaining its ultimate tensile strength then underwent strain softening until it could no longer bear the applied load at a tensile stress and strain of 4.6N/mm^2 and 0.042 respectively. Critically comparison analysis of the FE dog-bone performance curve (Figure 6(a)) with the experimental dog-bone performance curve (Figure 6(a)) revealed that the stress-strain behaviour during strain softening immediately after attaining ultimate tensile strength was slightly different. Whereas the FE model exhibited smooth strain softening, the experimental specimen exhibited zig-zag strain softening; and this may be due to the unavoidable imperfection with experiment in terms of the specimen shape, load application and boundary conditions among many other experimental errors.

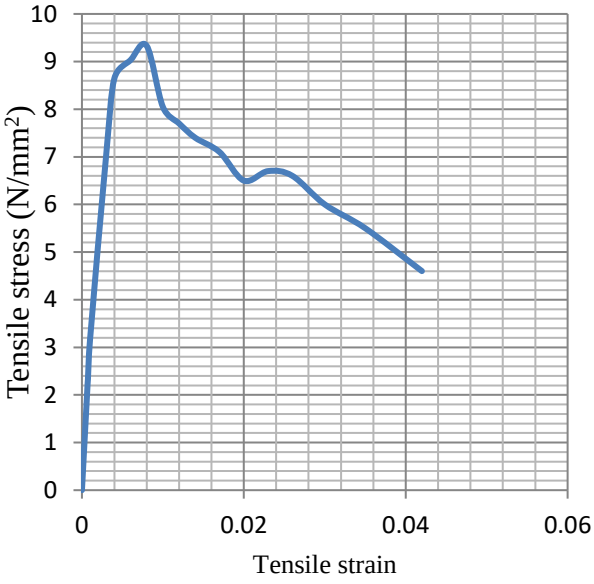

(a) FE dog-bone model's tensile stress-strain

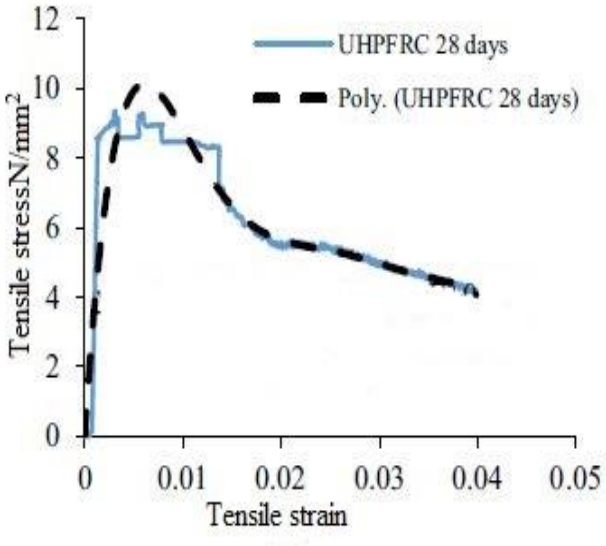

(b) Experimental tensile stress-strain (Hashim et al., 2020)

Figure 6. UHPFRCs' tensile stress-strain

The vertical direction stress of the prism shown through its contour in Figure 7(a) revealed that the vertical stresses were basically concentrated around the middle part of the prism with gradual distribution to other parts

of the prism. This vertical direction stress distribution may be the reason why the prism's crack pattern appeared the way it was in Figure 4(b). For the dog-bone specimen, the vertical direction stress contour presented in Figure 7(b) showed that the stresses were distributed around the same location within the notched section of the specimen where the ductile damage of the UHPFRC occurred. This stress contour of the specimen densely concentrated close to the loaded end section means that there is low rate of distribution to other part of the specimen; and this may be the reason while the tensile stress-strain performance curve of the FE dog-bone specimen shown in Figure 6(a) failed to exhibit ductile failure through strain hardening.

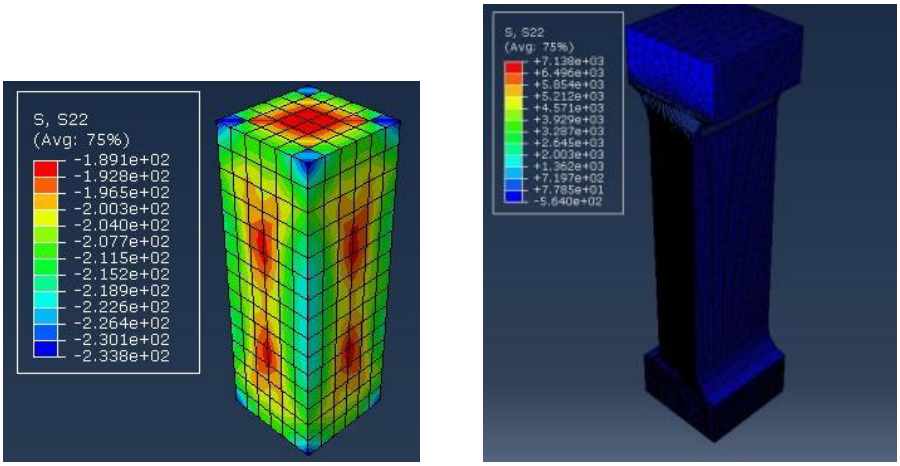

(a) Prism (b) Dog-bone

Figure 7. UHPFRC specimens' vertical stress contour

4. Conclusion

This study used ABAQUS package to model and simulate the strength properties of UHPFRC with micro and hooked-ends steel fibers; and the conclusions drawn from the compressive and tensile performance of the simulated specimens are presented as follows:

(1) The surface of the UHPFRC specimens remained largely un-damaged even after the applied load exceeded their ultimate compressive and tensile strength.

(2) The FE UHPFRC cube has an ultimate compressive strength of 260N/mm^2, about 7% higher than the experimental strength

(3) The FE prism specimen exhibited linear stress-strain behaviour up to 89% of its peak strength as well as non-linear stress-strain behaviour with both strain hardening and strain softening.

(4) The FE dog-bone specimen despite having ultra-high tensile strength did not undergo strain hardening phase as the vertical direction stresses were mainly distributed around the loaded section of the specimen.

(5) The FE specimens only had slight deviations from the experimental specimens in terms of ultimate compressive and tensile strength.

(6) The overall behaviour of the FE specimens in terms of deformation and strength performance are in perfect agreement with the experimental specimens. So FE modelling and simulation can be used to conduct extensive studies on UHPFRC properties and performances.

References

AFGC, (2002). French interim recommendations of ultra-high performance fiber reinforced concrete (UHPFRC), Paris: French Association of Civil Engineers.

ASTM C39/C39M, (2014). Standard test method for compressive strength of cylindrical concrete specimens, West Conshohocken: American Society for Testing and Materials International.

Azmee N M, Shafiq N, (2018). Ultra-high performance concrete: from fundamental to applications. *Case Studies in Construction Materials*, *9*, pp. 1-15. https://doi.org/10.1016/j.cscm.2018.e00197.

Bahraq A A, Al-Osta M A, Ahmad S, Al-Zahrani M M, Al-Dulaijan S O, Rahman M K, (2019). Experimental and numerical investigation of shear behavior of RC beams strengthened by ultra-high performance concrete. *International Journal of Concrete Structures and Materials*, *13*(6), pp. 1-19. https://doi.org/10.1186/s40069-018-0330-z.

Birtel V, Mark P, (2006). Parameterised finite element modelling of RC beam shear failure. *Proceedings of 2006 ABAQUS users' conference*, pp. 95-108.

Chowdhury M A, Islam M M, Zahid Z I, (2016). Finite element modelling of compressive and splitting tensile behavior of plain concrete and steel fibre reinforced concrete cylinder specimens. *Advances in Civil Engineering, 2016*(6579434), pp. 1-11. https://doi.org/10.1155/2016/6579434.

El-Helou R G, Haber Z B, Graybeal B A, (2022). Mechanical behaviour and design properties of ultra-high performance concrete. *ACI Materials Journal, 119*(1), pp. 181-194.

Graybeal B A, Baby F, (2013). Development of a direct tension test method for UHPFRC. *ACI Materials Journal, 110*, pp. 177-186.

Hashim D T, Hajezi F, Lei V Y, (2020). Simplified constitutive and damage plasticity models for UHPFRC with different types of fiber. *International Journal of Concrete Structures and Materials, 14*(45), pp. 1-21. https://doi.org/10.1186/s40069-020-00418-9.

Krahl P A, Carrazedo R, El Debs M K, (2018). Mechanical damage evolution in UHPFRC: experimental and numerical investigation. *Engineering Structures, 170*, pp. 63-77. https://doi.org/10.1016/j.engstruct.2018.05.064.

Lubliner J, Oliver J, Oller S, Onate E, (1989). A plastic-damage model for concrete. *International Journal of Solids and Structures*, vol. 25 no. 3, pp. 299-326.

Naeimi N, Moustafa M, (2019). Uniaxial compression behavior of ultra-high performance concrete confined by steel spirals. *Proceedings of the 2nd International Interactive Symposium on UHPC*, Albany, New York, United States, pp. 1-8.

Prem P R, Bharatkumar B H, Iyer N R, (2012). Mechanical properties of ultra-high performance concrete. *World Academy of Science, Engineering and Technology International Journal of Civil and Environmental Engineering, 6*(8), pp. 676-685.

Raja L V N, Sujatha T, (2014). Study on properties of modified reactive powder concrete. *International Journal of Engineering Research and Technology, 3*(10), pp. 937-940.

Rossi P, Arca A, Parant E, Fakhri P, (2004). Bending and compressive behaviors of a new cement composite. *Cement and Concrete Research*, *35*, pp. 27-33.

Sadrekarimi A, (2004). Development of light weight reactive powder concrete. *Journal of Advanced Concrete Technology, 2*(3), pp. 409-417.

Shi Z, Su Q, Kavoura F, Veljkovic M, (2023). Uniaxial tensile response and tensile constitutive model of ultra-high performance concrete containing coarse aggregate (CA-UHPC). *Cement and Concrete Composites, 136*(104878), pp. 1-17. https://doi.org/10.1016/j.cemconcomp.2022.104878.

Tao Y, Chen J, (2015). Concrete damage plasticity model for modelling FRP-to-concrete bond behaviour. *Journal of Composites for Construction, 19*(1), pp. 1-13.

Tian X, Fang Z, Zhou T, Xiang Y, (2023). Behavior and constitutive model of ultra-high-performance concrete under monotonic and cyclic tensile loading. *Construction and Building Materials, 389*(131634), pp. 1-22. https://doi.org/10.1016/j.conbuildmat.2023.131634.